Earth and Planetary Science Letters 294 (2010) 8–18

Contents lists available at ScienceDirect

Earth and Planetary Science Letters

journal homepage: www.elsevier.com/locate/epsl

Fe, C, and O isotope compositions of banded iron formation carbonates demonstrate a major role for dissimilatory iron reduction in ~2.5 Ga marine environments

Adriana Heimann [a,b,c,*], Clark M. Johnson [a,b], Brian L. Beard [a,b], John W. Valley [a,b], Eric E. Roden [a,b], Michael J. Spicuzza [a,b], Nicolas J. Beukes [d]

[a] University of Wisconsin, Department of Geoscience, 1215 West Dayton Street, Madison, WI 53706, USA
[b] NASA Astrobiology Institute, USA
[c] East Carolina University, Department of Geological Sciences, 101 Graham Building, Greenville, NC 27858, USA
[d] University of Johannesburg, Department of Geology, Johannesburg, South Africa

ARTICLE INFO

Article history:
Received 11 August 2009
Received in revised form 8 February 2010
Accepted 9 February 2010
Available online 1 April 2010

Editor: R.D. van der Hilst

Keywords:
Fe
isotopes
BIF
Kuruman
carbonates
Archean/Paleoproterozoic

ABSTRACT

Combined Fe, C, and O isotope measurements of ~2.5 Ga banded iron formation (BIF) carbonates from the Kuruman Iron Formation and underlying BIF and platform Ca–Mg carbonates of the Gamohaan Formation, South Africa, constrain the biologic and abiologic formation pathways in these extensive BIF deposits. Vertical intervals of up to 100 m were sampled in three cores that cover a lateral extent of ~250 km. BIF Fe carbonates have significant Fe isotope variability (δ^{56}Fe = +1 to −1‰) and relatively low δ^{13}C (down to −12‰) and δ^{18}O values (δ^{18}O ~ +21‰). In contrast, Gamohaan and stratigraphically-equivalent Campbellrand Ca–Mg carbonates have near-zero δ^{13}C values and higher δ^{18}O values. These findings argue against siderite precipitation from seawater as the origin of BIF Fe-rich carbonates. Instead, the C, O, and Fe isotope compositions of BIF Fe carbonates reflect authigenic pathways of formation in the sedimentary pile prior to lithification, where microbial dissimilatory iron reduction (DIR) was the major process that controlled the C, O, and Fe isotope compositions of siderite. Isotope mass-balance reactions indicate that the low-δ^{13}C and low-δ^{18}O values of BIF siderite, relative to those expected for precipitation from seawater, reflect inheritance of C and O isotope compositions of precursor organic carbon and ferric hydroxide that were generated in the photic zone and deposited on the seafloor. Carbon–Fe isotope relations suggest that BIF Fe carbonates formed through two end-member pathways: low-δ^{13}C, low-δ^{56}Fe Fe carbonates formed from remobilized, low-δ^{56}Fe aqueous Fe^{2+} produced by partial DIR of iron oxide, whereas low-δ^{13}C, high-δ^{56}Fe Fe carbonates formed by near-complete DIR of high-δ^{56}Fe iron oxides that were residual from prior partial DIR. An important observation is the common occurrence of iron oxide inclusions in the high-δ^{56}Fe siderite, supporting a model where such compositions reflect DIR "in place" in the soft sediment. In contrast, the isotopic composition of low-Fe carbonates in limestone/dolomite may constitute a record of seawater environments, although our petrographic studies indicate that the presence of pyrite in most low-Fe carbonates may influence the Fe isotope compositions. The combined Fe, C, and O isotope data from Kuruman BIF carbonates indicate that BIF siderites that have negative, near-zero, or positive δ^{56}Fe values may all record biological Fe cycling, where the range in δ^{56}Fe values records differential Fe mobilization via DIR in the sediment prior to lithification. Our results demonstrate that the inventory of low-δ^{56}Fe marine sedimentary rocks of Neoarchean to Paleoproterozoic age, although impressive in volume, may represent only a minimum of the total inventory of Fe that was cycled by bacteria.

1. Introduction

Interpretations of the isotopic compositions of ancient marine sedimentary rocks often divide into two groups; one, where these compositions are taken to reflect direct proxies for ancient seawater, and a second, where early authigenic mineral formation and soft-sediment diagenesis are thought to control the measured isotopic compositions. An example of these contrasting interpretations can be found in the Fe isotope record of Archean and Proterozoic marine sedimentary rocks. Rouxel et al. (2005) and Anbar and Rouxel (2007) interpret the Fe isotope compositions to directly reflect those of ancient seawater and call upon abiologic processes involving extensive precipitation of iron oxides to produce the negative δ^{56}Fe excursion in rocks of Neoarchean to Paleoproterozoic age, whereas Yamaguchi et al. (2005) and Johnson et al. (2008a,b) do not generally interpret the Fe isotope compositions to be a direct proxy for seawater and instead favor microbial iron cycling in the soft sediment prior to lithification as an

* Corresponding author. East Carolina University, Department of Geological Sciences, 101 Graham Building, Greenville, NC 27858, USA. Tel.: +1 252 328 5206; fax: +1 252 328 4391.
E-mail address: heimanna@ecu.edu (A. Heimann).

0012-821X/$ – see front matter © 2010 Elsevier B.V. All rights reserved.
doi:10.1016/j.epsl.2010.02.015

explanation for the Fe isotope variability. This debate echo's one that has existed for several decades in the literature on C isotopes, where the highly negative $\delta^{13}C$ values for iron formation carbonates have been interpreted by some studies to record microbial oxidation of organic matter (Becker and Clayton, 1972; Baur et al., 1985; Beukes and Gutzmer, 2008; Fischer et al., 2009), whereas other studies called upon an ocean that was stratified in C isotope compositions to explain the data (Beukes et al., 1990; Winter and Knauth, 1992; Klein, 2005).

Studies of iron formations, including banded iron formations (BIFs), provide an important test of the different interpretations for the major Fe isotope excursion towards negative Fe isotope compositions (Fig. 1) in ~2.7 to 2.4 Ga marine sedimentary rocks, because Fe-rich rocks place important mass-balance constraints on processes that may fractionate Fe isotopes. Periods of BIF deposition represent times when marine Fe fluxes were very high, including very high rates of Fe-rich sediment deposition, dramatically different than those of the modern marine iron cycle (Trendall, 2002; Trendall et al., 2004; Klein, 2005). Possible Fe pathways for producing the large inventories of Fe^{3+} in BIFs include oxidation of hydrothermal or riverine Fe^{2+} through reaction with O_2 produced by oxygenic photosynthesis (e.g., Cloud, 1968), or Fe^{2+} oxidation that was metabolically coupled to reduction of CO_2 (Konhauser et al., 2002; Kappler et al., 2005). Magnetite and siderite are the major Fe-bearing minerals in Late Archean to Early Proterozoic BIFs that have not been subjected to ore-forming processes or significant metamorphism. These Fe^{2+}-bearing minerals may have inorganically precipitated from an Fe^{2+}-rich ocean, but they are also common end products of dissimilatory iron reduction (DIR) (Lovley et al., 1987), and a role for DIR in BIF genesis has been proposed by Walker (1984), Nealson and Myers (1990), Lovley (1991), and Konhauser et al. (2005); DIR is known to be a deeply rooted metabolism in both Bacteria and Archaea (Vargas et al., 1998; Lovley, 2004), and hence some evidence for this metabolism is likely in the ancient rock record.

In this contribution, we analyze Fe, C, and O isotope compositions in BIF carbonates siderite and ankerite from the ~2.5 Ga Kuruman Iron Formation, South Africa. Through detailed petrographic, chemical, and isotopic analysis, including Fe, C, and O isotope determinations on the same millimeter-scale iron formation carbonates, and comparison to coeval Ca–Mg carbonates, we argue here that distinct biologic and abiologic pathways may be determined. These results, in turn, provide strong constraints on the inventory of Fe in BIFs that was cycled by biological processes, and permit a critical evaluation of the importance of microbial Fe metabolisms in the ancient marine sedimentary rock record.

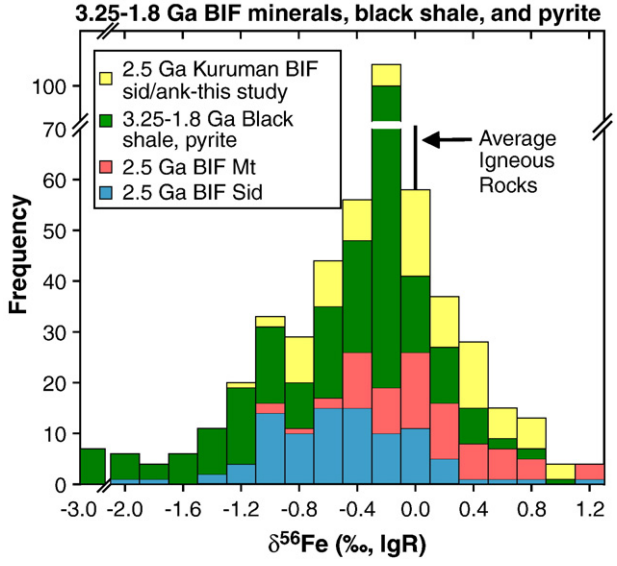

Fig. 1. Histogram showing the Fe isotope composition ($\delta^{56}Fe$, in ‰, relative to igneous rocks) of ~2.5 Ga BIF minerals (magnetite and siderite) and 3.25 to 1.8 Ga black shale and pyrite. Data from other studies are from Johnson et al. (2003), Yamaguchi et al. (2005), Rouxel et al. (2005), Archer and Vance (2006), and Johnson et al. (2008a). Shown for comparison is the average $\delta^{56}Fe$ of igneous rocks from Beard et al. (2003a). The histogram also includes new data for siderite- and ankerite-rich carbonates from the ~2.5 Ga Kuruman Iron Formation, Transvaal, South Africa, obtained in this study.

2. Geology, sample selection, and analytical methods

The ~2.5 Ga Kuruman and Gamohaan BIFs, Transvaal Craton, South Africa, are the best preserved examples of Archean/Proterozoic carbonate BIF, and they have been correlated with the Brockman and Weelli Wolli iron formations of the Hamersley Basin, Western Australia (Cheney, 1996; Beukes and Gutzmer, 2008). The Kuruman BIF was subjected to a very low degree of deformation and metamorphism (T = 110–170 ºC, P<2 kbar; Miyano and Beukes, 1984). Beukes et al. (1990) and Klein and Beukes (1989) defined siderite-, magnetite-, and Fe silicate-rich BIF facies, all of which contain variable amounts of chert. The samples analyzed in this study came exclusively from the siderite-rich facies layers of the Kuruman BIF, from three stratigraphically-equivalent drill cores, DI-1, AD-5, and WB-98 (Fig. 2; Klein and Beukes, 1989). The sequence of rocks records a transition from limestone/dolomite platform carbonates of the lower Gamohaan Formation through the BIFs of the upper Gamohaan Formation (Tsineng Member or "Bruno's BIF"; Beukes and Gutzmer, 2008), to the Fe carbonate-rich BIF of the Kuruman Iron Formation (Klein and Beukes, 1989). The BIF package was deposited over a period of 1.08 to 3.25 million years, based on calculated sedimentation rates for the Kuruman BIF (e.g., Altermann and Nelson, 1998). The cores studied here represent BIF deposition in the shallower parts of the Transvaal basin (Beukes et al., 1990; Beukes and Gutzmer, 2008).

One hundred samples of carbonate laminations were obtained from the Kuruman BIF and underlying Gamohaan BIF, limestone, and dolomite, following detailed petrographic study of a larger sample set. We emphasize that milligram-size samples were analyzed because it was important to maintain a small sample size in these finely laminated sediments. Major-element chemistry and modal mineralogy were determined by electron microprobe and scanning electron microscope (SEM) analysis. Iron, carbon, and oxygen isotope compositions were determined using standard methods, and reported as $\delta^{56}Fe$, $\delta^{13}C$, and $\delta^{18}O$ values, respectively. See the Appendix for details.

3. Petrography and mineral chemistry

Zones of Fe-rich carbonate commonly coexist with chert, or are interlaminated with carbonate-bearing chert. Most BIF carbonate laminations contain siderite ($FeCO_3$) and ankerite ($[Ca,Fe,Mg]CO_3$) in different proportions (Tables S1, S3). Siderite is, in most cases, very fine-grained (~5 μm), but also occurs as fine-grained individual subhedral rhombohedral crystals (~10 μm in size). Ankerite is coarser grained (~>30 μm) than siderite and contains abundant siderite inclusions, indicating that it formed after siderite (Fig. 3A, B). We found trace amounts of minute (<1 μm) Fe-oxide inclusions in ankerite and siderite, identified as hematite (Fe_2O_3) based on petrographic analysis (red color of larger crystals under plane-polarized light, anisotropic under crossed-polarized light) and energy dispersive spectrometry (EDS) spectra (Fig. 3A, B; Fig. S1); the common occurrence of hematite inclusions in siderite forms an important clue to Fe pathways, as will be discussed below. In addition, preliminary electron back-scattered diffraction (EBSD) and transmission electron microscope (TEM) analysis shows that some of the iron oxide inclusions are nano-size magnetite. Only trace amounts of pyrite, stilpnomelane, and greenalite are present in a small number of the samples selected for study (Fig. 3C; Table S1). Limestone and dolomite from the Gamohaan Formation commonly contain coexisting calcite and ferroan dolomite (Fig. 3D). Although areas that contained Fe-bearing phases other than carbonate were avoided, pyrite is a common inclusion in a number of samples (Fig. 3D). The

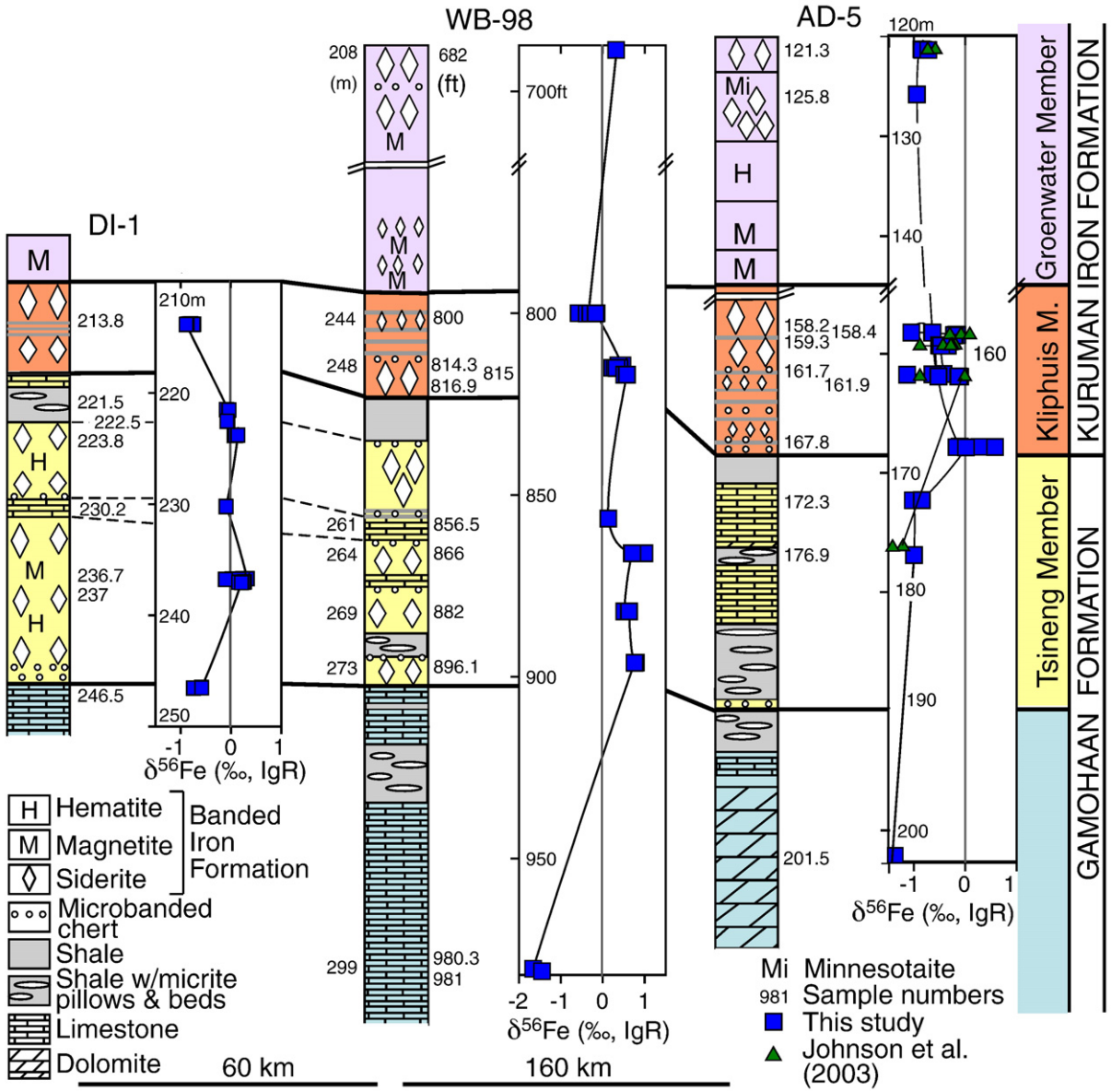

Fig. 2. Simplified lithostratigraphic profiles and corresponding Fe isotope profiles for cores DI-1, WB-98, and AD-5. The sequence of rocks encompasses the ~2.5 Ga transition from the carbonate platform of the Gamohaan Formation to the Kuruman Iron Formation, Transvaal basin, South Africa. Iron isotope compositions are expressed as δ^{56}Fe in units of per mil (‰, relative to igneous rocks). Note the difference in δ^{56}Fe scales. Lithostratigraphy modified from Klein and Beukes (1989). Similar profiles with corresponding carbon and oxygen isotope data are shown in the Appendix (Figs. S4, S5).

compositions of coexisting ankerite and siderite in BIFs, and calcite and ferroan dolomite in limestone and dolomite, are shown in Fig. 4 (Table S3). Based on image analysis and mineral compositions, the Fe budget in siderite–ankerite samples and in most calcite/dolomite samples is dominated by the carbonate (Fig. S3).

4. Isotopic compositions

Oxygen ($\delta^{18}O_{SMOW}$) and carbon ($\delta^{13}C_{PDB}$) isotope compositions for BIF carbonate vary from +19 to +21‰ SMOW and −2.6 to −12‰ PDB, respectively, and overlap the range measured for siderite-facies BIF in the Campbellrand–Kuruman stratigraphy by Beukes et al. (1990), Beukes and Klein (1990), Kaufman (1996), and Fischer et al. (2009). Oxygen isotope compositions for iron carbonates in oxide- and Fe silicate-facies BIFs of the Gamohaan and Kuruman formations determined by Beukes et al. (1990), Beukes and Klein (1990), and Kaufman (1996), however, extend to significantly lower δ^{18}O values, as low as +16‰, and these facies also tend to have the lowest δ^{13}C values (Fig. 5A). In contrast, δ^{18}O values for Ca–Mg carbonates in the Gamohaan Formation (Beukes et al., 1990; Beukes and Klein, 1990; Kaufman, 1996) and stratigraphically-equivalent Campbellrand platform rocks (Fischer et al., 2009) have significantly higher δ^{18}O values, generally between +21 and +24‰, and δ^{13}C values cluster around −1.0‰ (Fig. 5A; Table S1 and Figs. S4–S8).

Iron isotope compositions (δ^{56}Fe) in all the analyzed carbonates range from +1.0 to −1.7‰ (Fig. 5B), and overlap those determined by Johnson et al. (2003). The range in Fe isotope compositions measured here also overlaps that determined for Campbellrand Ca–Mg carbonates by von Blanckenburg et al. (2008). In contrast to the positive correlation between δ^{13}C and δ^{18}O for the carbonates, there is no correlation between δ^{56}Fe and δ^{18}O values for the BIF and Ca–Mg carbonates (Fig. 5B). There are, however, important relations between δ^{56}Fe values and carbonate composition and the nature of mineral inclusions (see Fig. 5B caption). Siderite–ankerite samples that contain magnetite and/or hematite inclusions are restricted to samples that have δ^{56}Fe>0‰, and ~2/3 of the siderites that have positive δ^{56}Fe

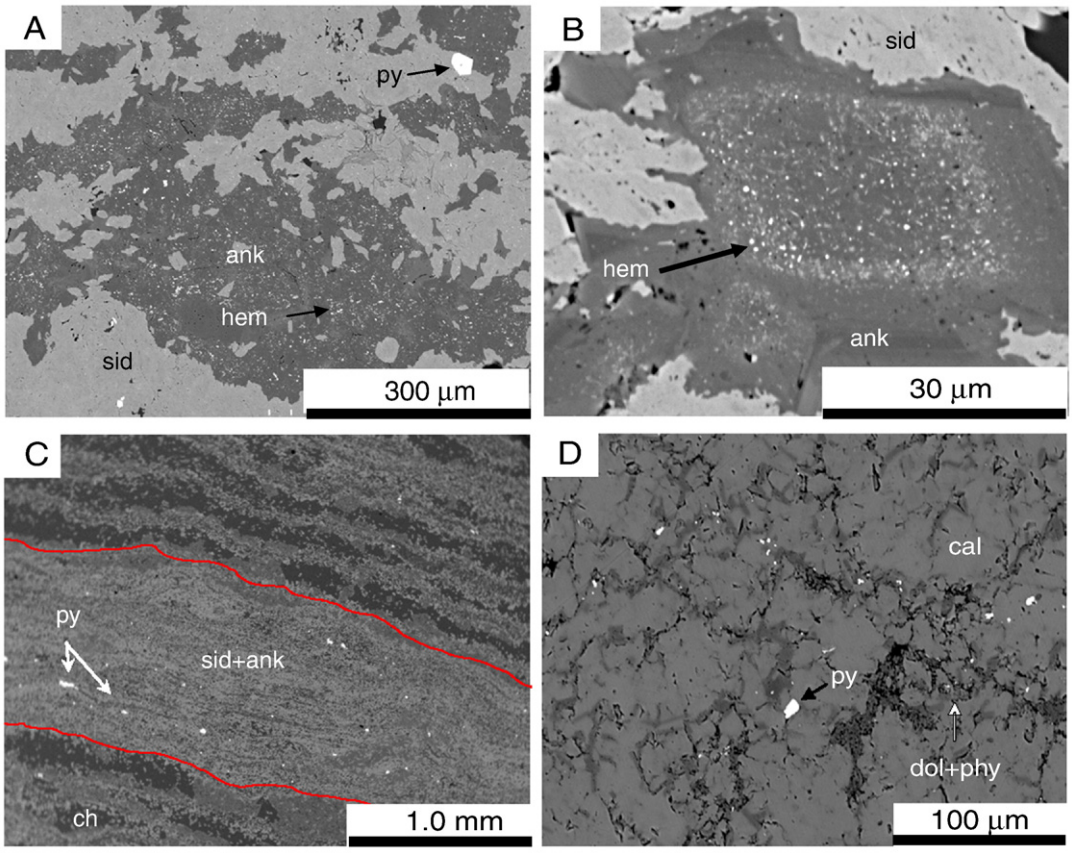

Fig. 3. Representative mineral relationships observed in carbonate-rich iron formation from the Kuruman Iron Formation and Gamohaan Formation, and limestone/dolomite from the Gamohaan Formation, as seen by back-scattered secondary electron microscope imaging. *A.* Iron oxide (hematite, hem) inclusions (bright white) in ankerite (dark grey, ank) and siderite (light grey, sid). The subhedral crystal is pyrite (py). Preliminary results indicate that some of the tiny Fe oxides are also nano-size magnetite. Sample DI1-237 m, lamination 8. *B.* Close-up of iron oxide (hematite, bright) and siderite inclusions (light grey) in ankerite (dark grey) surrounded by siderite. The black area is void space. Sample WB98-866B, lamination 3. *C.* Pyrite-bearing siderite–ankerite lamination. Siderite is light grey, ankerite is dark grey, and chert (ch) appears as very dark grey. Sample DI1-213.8mC, lamination 3. *D.* Limestone composed of calcite (cal), minor interstitial ferroan dolomite (dark grey, dol) and phyllosilicate (dark grey, phy), and accessory pyrite (bright). Sample AD-5-176.9 m, lamination 1.

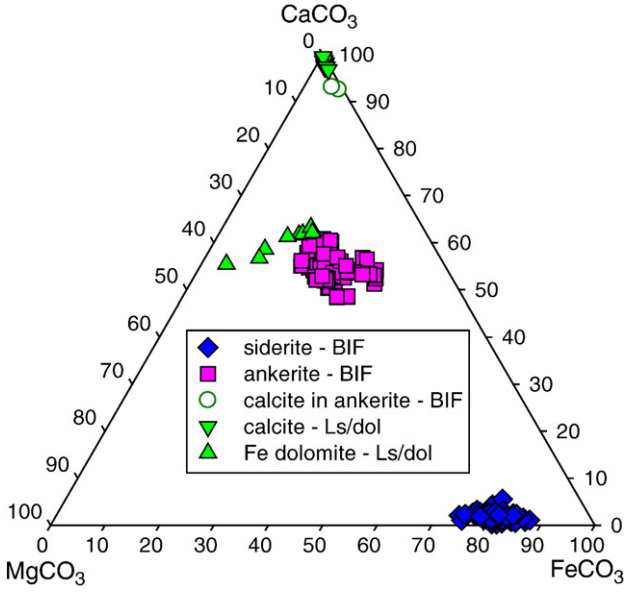

Fig. 4. Major-element compositions of individual carbonate minerals present in each lamination of carbonate from the Kuruman Iron Formation and limestone/dolomite from the transition from platform carbonate (Gamohaan Formation) to BIF, obtained by electron microprobe analysis and expressed in mol% siderite, calcite, and magnesite end-members (Table S3). Siderite, ankerite, and calcite in ankerite are from BIF samples. Calcite and Fe dolomite are from limestone and dolomite (Ls/dol).

values contain magnetite and/or hematite inclusions (Fig. 5B). It is important to note that despite the common occurrence of Fe-oxide inclusions in the δ^{56}Fe>0‰ siderite, in no case do the inclusions exert a significant effect on the measured Fe isotope composition of these Fe-rich carbonates (Fig. S3B). A group of siderite–ankerite samples that have δ^{56}Fe values ~−0.8‰ contain minor pyrite inclusions (Fig. 5A), although the proportion of Fe contained in pyrite, relative to that in siderite, is very low, only as high as 0.05% (Fig. S3A). About half of the calcite/dolomite samples analyzed contain pyrite inclusions, and, given the low Fe contents of these carbonates, pyrite may comprise up to 50% of the Fe budget of the material sampled (Fig. S3A), and therefore may have influenced the measured δ^{56}Fe values.

5. Discussion

We first discuss the C, O, and Fe isotope compositions measured in Fe-rich BIF and Ca–Mg carbonates in terms of isotopic equilibrium or disequilibrium with ancient seawater, as evaluated in light of theoretical and experimental isotopic fractionation factors. Based on this evaluation, we next discuss the possible reaction pathways associated with DIR, which predict specific C, O, and Fe isotope compositions distinct from those that would be produced by precipitation from seawater. Finally, we discuss the internal re-distribution of Fe that may occur in the soft sediment during authigenic mineral formation by DIR that can explain the range in measured Fe isotope compositions.

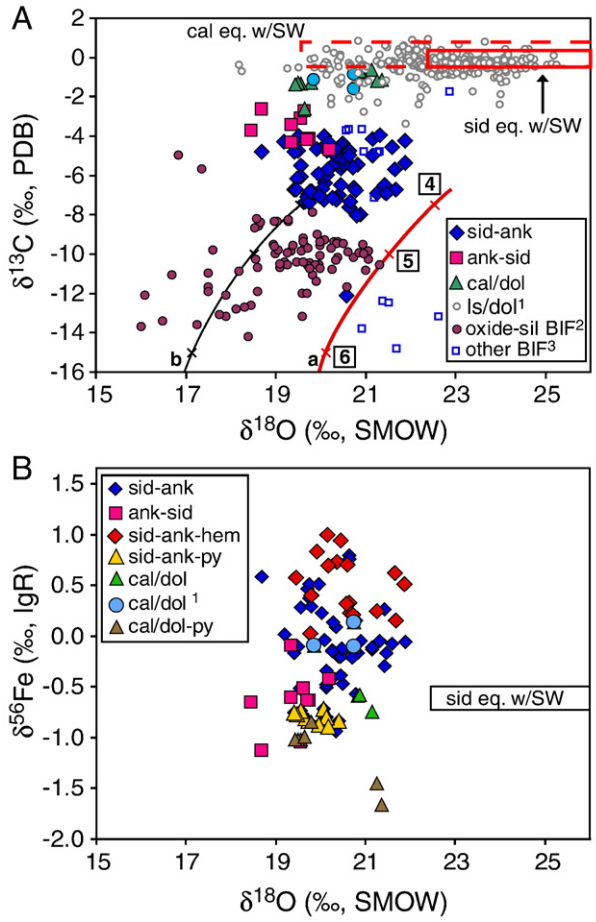

Fig. 5. Oxygen isotope composition ($\delta^{18}O$ in ‰, relative to SMOW) vs. C isotope composition ($\delta^{13}C$ in ‰, relative to PDB; *A*) and Fe isotope compositions ($\delta^{56}Fe$ in ‰, relative to igneous rocks; *B*) for millimeter-scale Kuruman and Gamohaan Formation BIF Fe carbonates and Gamohaan Formation limestone/dolomite. Large symbols indicate data from this study. Data in *B* are subdivided by the type of minor Fe-bearing phases present in the carbonate samples (i.e., hematite and pyrite), although for Fe-rich carbonates the Fe budget is dominated by the carbonate (see Fig. S3). 1 in B) are cal/dol samples from the Tsineng Member, Gamohaan Fm. Data from other studies are: [1]bulk-rock limestone and dolomite compositions from Beukes et al. (1990), Kaufman (1996), and Fischer et al. (2009); those from Fischer et al. (2009) are mostly dolomite; [2]bulk-rock samples of oxide- and silicate-facies BIF carbonate from Beukes et al. (1990) and Kaufman (1996); and [3]bulk-rock carbonate samples of other BIF from Fischer et al. (2009). Curves "a" and "b" represent model compositions calculated using the equations in Table 1 and two $\delta^{18}O$ values for Archean/Proterozoic seawater: $^{a}\delta^{18}O$ for seawater = −1‰, and $^{b}\delta^{18}O$ for seawater = −4‰. The numbers on the curves denote compositions from the respective equations in Table 1. The rectangles in *A* and *B* show the isotopic compositions of siderite and calcite in equilibrium with seawater calculated from 25 °C to 50 °C using the $\Delta^{18}O$ fractionation factors for siderite–H_2O and calcite–H_2O of Carothers et al. (1988) and Kim and O'Neil (1997), respectively, $\Delta^{56}Fe$ for Fe^{2+}–siderite from Wiesli et al. (2004), $\delta^{13}C$ of seawater = 0‰, and the two $\delta^{18}O$ values for seawater noted above. Mineral abbreviations are the same as in previous figures.

5.1. Isotopic disequilibrium with seawater

Virtually none of the siderites analyzed in this study have C, O, and Fe isotope compositions that match those expected for equilibrium precipitation from a common Neoarchean or Paleoproterozoic seawater (Fig. 5A, B). Only the calcite and dolomite samples have the near-zero $\delta^{13}C$ values that are common for Ca–Mg carbonates of this age (Shields and Veizer, 2002), which are interpreted to reflect direct precipitation from seawater. Because the fractionation factor for carbon isotopes between siderite and calcite ($\Delta^{13}C_{siderite-calcite}$) is ~ −0.5‰ at room temperature (Jimenez-Lopez et al., 2001; Jimenez-Lopez and Romanek, 2004), siderite and calcite should have similar $\delta^{13}C$ values if they precipitated in equilibrium with DIC from a common seawater. The differences in $\delta^{18}O$ values among the different carbonates analyzed in these rocks (calcite/dolomite, ankerite, and siderite) cannot be explained by equilibrium O isotope fractionation factors if they precipitated from a common fluid. The contrast in the $\Delta^{18}O_{calcite-water}$ (Kim and O'Neil, 1997) and $\Delta^{18}O_{siderite-water}$ (Carothers et al., 1988) fractionation factors at room temperature indicates that siderite should be ~4‰ higher in $\delta^{18}O$ than calcite if these minerals precipitated from a common fluid. In contrast, the $\delta^{18}O$ values for siderite in siderite-facies BIF are, on average, ~2 to 3‰ lower than temporally equivalent Ca–Mg carbonates of the Campbellrand–Kuruman sequence, and the contrast is even larger, up to 9‰, when considering siderite in oxide-facies BIF (Fig. 5A); assuming a common fluid, such contrasts would require precipitation temperatures >100 °C higher for siderite. The contrast in $\delta^{18}O$ values cannot be explained through metamorphic re-equilibration, as indicated by independent evidence that metamorphism in the rocks studied did not exceed 170 °C (Miyano and Beukes, 1984), and the relatively low $\delta^{18}O$ values for siderite are unlikely to reflect recrystallization through interaction with meteoric water, given the petrographic evidence for early primary textures in siderite and the fact that interbedded cherts have high $\delta^{18}O$ values (Kaufman, 1996).

The majority of BIF siderites analyzed in this study do not have $\delta^{56}Fe$ values that are expected to reflect those in equilibrium with Neoarchean or Paleoproterozoic seawater (Fig. 5B), a conclusion reached by Johnson et al. (2008a) in their study of siderite from the broadly correlative Dales Gorge Member of the Brockman Iron Formation, Australia. Moreover, the small-scale Fe isotope variability measured millimeters to centimeters apart also suggests that the BIF Fe carbonates could not have precipitated in isotopic equilibrium with seawater, given the long residence time expected for an Fe^{2+}-rich ocean (Johnson et al., 2008a). Neoarchean or Paleoproterozoic seawater that had high concentrations of Fe^{2+}_{aq} probably had $\delta^{56}Fe$ values between −0.2 and 0.0‰ (Yamaguchi et al., 2005; Johnson et al., 2008b). As noted by Johnson et al. (2008a), Fe-poor regions of the oceans, such as the photic zone, could have had significantly negative $\delta^{56}Fe$ values, but siderite would be an unlikely precipitate from such seawater. Based on these estimates for Fe-rich seawater, and the Fe^{2+}_{aq}–siderite $^{56}Fe/^{54}Fe$ fractionation factor of 0.5‰ of Wiesli et al. (2004), siderite that precipitated in equilibrium with Neoarchean or Paleoproterozoic seawater would be expected to have a $\delta^{56}Fe$ value between −0.5 and −0.7‰. The conclusion that BIF siderites that have $\delta^{56}Fe$ values > −0.5‰ cannot reflect precipitation from seawater holds if alternative Fe^{2+}_{aq}–siderite $^{56}Fe/^{54}Fe$ fractionation factors are used instead of that of Wiesli et al. (2004); combining the calculated $\beta^{56/54}$ factors available for Fe^{2+}_{aq} (Schauble et al., 2001; Anbar et al., 2005; Domagal-Goldman and Kubicki, 2008) with the calculated $\beta^{56/54}$ factor for siderite of Polyakov and Mineev (2000) produces Fe^{2+}_{aq}–siderite fractionations that are 1.1 to 2.2‰ higher than the experimentally determined fractionation of Wiesli et al. (2004). These calculations make it even more difficult to explain the $\delta^{56}Fe$ values for BIF siderite that are > −0.5‰ through equilibrium with seawater.

5.1.1. Stratified seawater?

If the C, O, and Fe isotope variations do not permit inorganic precipitation from a common fluid, could the data be interpreted to reflect precipitation from seawater that was stratified in $\delta^{13}C$, $\delta^{18}O$, and $\delta^{56}Fe$ values? Previous studies on identical or correlative rock sections as the one studied here have been interpreted to reflect stratification in C-, S-, Fe- and Nd-isotopes, in part based on seawater-like REE-Y compositions for carbonates (e.g., Klein and Beukes, 1989; Beukes et al., 1990; Kamber and Webb, 2001; Kamber and Whitehouse, 2007; von Blanckenburg et al., 2008). The variability seen in C isotope compositions throughout the stratigraphy from $\delta^{13}C$ values near zero for Ca–Mg carbonates of the Gamohaan Formation to lower $\delta^{13}C$ values for younger BIF samples (Fig. S4 core WB-98), documented here and in previous work (Klein and Beukes, 1989; Beukes et al.,

1990), could be interpreted to reflect a shift to negative $\delta^{13}C$ values for dissolved inorganic carbon (DIC) during deepening of the basin. A closer inspection of the stratigraphic and isotopic profiles, however, shows this apparent trend to be mineral-dependent, where siderite, which has the most negative $\delta^{13}C$ values of the various carbonates, increases in abundance up section. As noted above, the mineralogic effect on $^{13}C/^{12}C$ fractionations is small for carbonates, and therefore these observations are inconsistent with a water column that was stratified in $\delta^{13}C$ values. Recent work by Fischer et al. (2009) documented no systematic difference in $\delta^{13}C$ values for shallow- and deep-water carbonates in similar-age samples from the Campbellrand–Kuruman platform, where $\delta^{13}C$ values of Neoarchean or Paleoproterozoic seawater were estimated to lie between −2 and 0‰. Based on C-flux modeling, Fischer et al. (2009) noted that large vertical $\delta^{13}C$ gradients in ancient seawater would suggest very high levels of productivity, which seems unlikely at ~2.5 Ga. We conclude, therefore, in agreement with current models for BIF formation (e.g., Beukes and Gutzmer, 2008), that the negative $\delta^{13}C$ values for Fe-rich BIF carbonates require other C sources in addition to DIC from seawater, and therefore cannot reflect seawater stratification in C isotope compositions.

A stratified ocean cannot explain the up to 9‰ range in $\delta^{18}O$ values for BIF carbonates (Fig. 5A). The maximum $\delta^{18}O$ gradient in modern restricted basins such as the Black Sea is ~4‰, where the lowest $\delta^{18}O$ values are found in surface waters, reflecting local meteoric input (e.g., Swart, 1991). Assuming an analogous relation to a Kuruman–Campbellrand restricted basin, the shallow water Ca–Mg carbonates would be expected to have $\delta^{18}O$ values lower than the deeper water, Fe-rich carbonates, opposite to the observed trends (Fig. 5). We stress that although there remains uncertainty in the paleotemperatures and O isotope compositions of Precambrian seawater (e.g., Knauth, 2005; Kasting et al., 2006), the relative trends in $\delta^{18}O$ values discussed here do not depend upon knowledge of the absolute $\delta^{18}O$ values or temperature of ancient seawater; we conclude, therefore, that the O, and C, isotope compositions of ankerite and siderite from the Kuruman BIF do not reflect direct formation from seawater, although the Ca–Mg carbonates appear likely to have formed by precipitation from seawater.

5.2. Biologic pathways for BIF siderite formation

If the C, O, and Fe isotope compositions for the BIF siderites studied here cannot be explained by direct precipitation from seawater, even from a stratified water column or restricted basin, we turn to authigenic and early diagenetic processes in the soft sediment prior to lithification as an explanation of the data. Most models for BIF formation call upon Fe^{2+}_{aq} oxidation and formation of ferric iron precipitates in the shallow oceans (e.g., Beukes et al., 1990; Klein, 2005). Oxidation of Fe^{2+} may occur indirectly by O_2 generated by photosynthesis:

$$CO_2 + H_2O \rightarrow CH_2O + O_2 \quad (1)$$

and

$$4Fe^{2+}_{aq} + O_2 + 8OH^- + 2H_2O \rightarrow 4Fe(OH)_3. \quad (2)$$

Eqs. (1) and (2) provide a flux of 1 mol of organic carbon (CH_2O) for every 4 mol of iron oxide ($Fe(OH)_3$) to the seafloor. Oxidation of hydrothermal Fe^{2+} may also occur by anaerobic phototrophy (e.g., Kappler et al., 2005):

$$4Fe^{2+}_{aq} + CO_2 + 11H2O \rightarrow 4Fe(OH)_3 + CH_2O + 8H, \quad (3)$$

which also provides a 1:4 flux of CH_2O and $Fe(OH)_3$ to the seafloor. A third oxidation pathway has been discussed in the literature, UV photo-oxidation (e.g., Cairns-Smith, 1978), although this has been recently shown to be unlikely in natural seawater compositions (Konhauser et al., 2007).

A flux of reactive iron oxide and organic carbon to the seafloor in Neoarchean oceans that had generally low levels of dissimilatory sulfate reduction (DSR) would have provided conditions highly favorable to DIR (Johnson et al., 2008b). Under conditions of complete iron oxide reduction, two sources of C are required for siderite formation:

$$4Fe(OH)_3 + CH_2O + 3HCO_3^- \rightarrow 4FeCO_3 + 3OH^- + 7H_2O. \quad (4)$$

The most abundant source of HCO_3^- would come from seawater infiltration into the soft sediment, below the seawater/sediment interface. If HCO_3^- is not present in excess, complete reduction will produce Fe^{2+}_{aq} in addition to siderite:

$$4Fe(OH)_3 + CH_2O + 2HCO_3^- \rightarrow 3FeCO_3 + Fe^{2+}_{aq} + 4OH^- + 6H_2O \quad (5)$$

Or, using a different CH_2O:HCO_3^- ratio,

$$4Fe(OH)_3 + CH_2O + HCO_3^- \rightarrow 2FeCO_3 + 2Fe^{2+}_{aq} + 5OH^- + 5H_2O. \quad (6)$$

If no external source of HCO_3^- is available, complete reduction may be written as:

$$4Fe(OH)_3 + CH_2O \rightarrow FeCO_3 + 3Fe^{2+}_{aq} + 6OH^- + 4H_2O. \quad (7)$$

If excess $Fe(OH)_3$ is available relative to CH_2O, the excess Fe^{2+}_{aq} produced in Eq. (7) may result in magnetite formation:

$$3Fe^{2+}_{aq} + 6OH^- + 6Fe(OH)_3 \rightarrow 3Fe_3O_4 + 12H_2O. \quad (8)$$

Similar reactions may be written for magnetite formation accompanying Eqs. (5) and (6).

The stoichiometries of Eqs. (4)–(7) predict specific C, O, and Fe isotope variations for siderite that are distinct from those produced by precipitation from seawater (Table 1). We assume organic carbon (CH_2O) input to the seafloor had a $\delta^{13}C$ value of −30‰, based on the average $\delta^{13}C$ value for organic carbon in the 2.5 Ga Campbellrand–Kuruman carbonates (Beukes et al., 1990; Kaufman, 1996; Fischer et al., 2009). The isotopic composition of DIC (HCO_3^-) in seawater is assumed to have a $\delta^{13}C$ value of 0‰, where no vertical gradient existed in the water column, based on the results of Fischer et al. (2009). For complete $Fe(OH)_3$ reduction and complete utilization of organic carbon with no production of excess Fe^{2+}_{aq} (Eq. (4)), the lowest possible $\delta^{13}C$ value is ~−7.5‰ for siderite whose Fe has been entirely processed by DIR. The majority of $\delta^{13}C$ values for siderite in siderite-facies BIF scatter about the $\delta^{13}C$ value predicted by Eq. (4), consistent with the large proportion of Fe carbonate produced by Eq. (4) relative to other Fe products.

The O isotope compositions of siderite produced by DIR are expected to deviate strongly from those produced by precipitation from seawater, where decreasing $\delta^{18}O$ values will accompany decreasing $\delta^{13}C$ values, using the constraints imposed by Eqs. (4) through (7) (Table 1). We illustrate two relations between $\delta^{18}O$ and $\delta^{13}C$ for siderite produced by DIR based on two assumed $\delta^{18}O$ values for Neoarchean and Paleoproterozoic seawater. One set of calculations assumes a seawater $\delta^{18}O$ of −1‰, essentially a modern, ice-free ocean value (Muehlenbachs, 1998), and a second set assumes a $\delta^{18}O$ value of −4‰, a conservative alternative value that lies midway between that of modern seawater and that predicted by Kasting et al. (2006) for seawater at ~2.5 Ga. The decreasing $\delta^{18}O$ values for siderite produced by Eqs. (4) through (7) reflect an increasing contribution of O from the precursor $Fe(OH)_3$ produced in the photic zone (Table 1), using the $\Delta^{18}O_{\text{ferric hydroxide–water}}$ fractionation factors of −1‰ of Bao and Koch (1999) and Bao et al. (2000). The $\delta^{13}C$–$\delta^{18}O$ relations predicted by Eqs. (4) through (7), when a modest range in possible $\delta^{18}O$ values for seawater is considered, encompass most of the data for BIF siderite in the current and previous studies (Fig. 5A), and predict that the lowest $\delta^{13}C$ and $\delta^{18}O$ values for siderite should occur in oxide- and Fe silicate-facies BIF, where excess

Table 1
Fe–C–O isotope mass-balance reaction pathways for siderite formation via DIR.

Eq. (4)	$4Fe(OH)_3$	$+ CH_2O$	$+ 3HCO_3^-$	→	$4FeCO_3$	$+ 3OH^-$	$+ 7H_2O$	
δ^{56}Fe (‰)	0.00				0.00			
δ^{13}C (‰)		−30.0	0.0		−7.5			
δ^{18}O (‰)[a]	−2.0	−1.0	29.0		22.6		−3.5	
δ^{18}O (‰)[b]	−5.0	−4.0	26.0		19.6		−6.5	
Eq. (5)	$4Fe(OH)_3$	$+ CH_2O$	$+ 2HCO_3^-$	→	$3FeCO_3$	$+ 4OH^-$	$+ 6H_2O$	$+ Fe^{2+}$
δ^{56}Fe (‰)	0.00				−0.13			0.38
δ^{13}C (‰)		−30.0	0.0		−10.0			
δ^{18}O (‰)[a]	−2.0	−1.0	29.0		21.5		−4.5	
δ^{18}O (‰)[b]	−5.0	−4.0	26.0		18.5		−7.5	
Eq. (6)	$4Fe(OH)_3$	$+ CH_2O$	$+ HCO_3^-$	→	$2FeCO_3$	$+ 5OH^-$	$+ 5H_2O$	$+ 2Fe^{2+}$
δ^{56}Fe (‰)	0.00				−0.25			0.25
δ^{13}C (‰)		−30.0	0.0		−15.0			
δ^{18}O (‰)[a]	−2.0	−1.0	29.0		20.1		−5.9	
δ^{18}O (‰)[b]	−5.0	−4.0	26.0		17.1		−8.9	
Eq. (7)	$4Fe(OH)_3$	$+ CH_2O$		→	$FeCO_3$	$+ 6OH^-$	$+ 4H_2O$	$+ 3Fe^{2+}$
δ^{56}Fe (‰)	0.00				−0.38			0.13
δ^{13}C (‰)		−30.0	0.0		−30			
δ^{18}O (‰)[a]	−2.0	−1.0	29.0		18.1		−7.9	
δ^{18}O (‰)[b]	−5.0	−4.0	26.0		15.1		−10.9	

Notes: Equation numbers correspond to those in the text and in Fig. 5A. Input isotope compositions are as follows: δ^{18}O correspond to two models calculated using different seawater isotopic compositions: [a]δ^{18}O sw = −1‰ (Muehlenbachs, 1998), and [b]δ^{18}O sw = −4‰ (Kasting et al., 2006), respectively; δ^{13}C for organic carbon = −30‰ (Fischer et al., 2009); δ^{13}C for DIC = 0‰; δ^{56}Fe for $Fe(OH)_3$ = 0‰. Fractionation factors used are as follows: $\Delta^{18}O_{Sid-H_2O}$ = 26‰ (50 °C; Carothers et al., 1988); $\Delta^{18}O_{HCO_3^- - H_2O}$ = 30‰ (20 °C; Beck et al., 2005); $\Delta^{18}O_{CH_2O-H_2O}$ = 0‰ (Guy et al., 1993); $\Delta^{18}O_{Fe(OH)_3-H_2O}$ = −1‰ (20 °C; Bao and Koch, 1999; Bao et al., 2000); $\Delta^{56}Fe_{Fe_{2+}-sid}$ = 0.5‰ (Wiesli et al., 2004). Siderite in equilibrium with seawater has δ^{13}C = 0‰ and δ^{18}O = +25‰ for [a] and δ^{18}O = +22‰ for [b].

Fe^{2+}_{aq} is produced (Eqs. (5) through (7)). Combined, the δ^{13}C and δ^{18}O values for BIF siderite provide strong evidence for DIR.

The very low organic carbon contents of BIFs, particularly in oxide-facies, have been used to argue against a biological role in BIF formation (e.g., Klein, 2005), or to support metamorphic formation of siderite or magnetite through reaction of organic carbon and iron oxides (e.g., Perry et al., 1973). Alternatively, the low organic carbon contents are consistent with a major role for DIR (together with later Fe mineral transformations) in BIF genesis, and DIR predicts that organic carbon contents should be correlated with δ^{13}C values for siderites in BIFs (Fig. S9), a relation that cannot be explained by abiologic reactions of organic carbon and iron oxide. Indeed, the fact that the lowest organic carbon contents (and lowest δ^{13}C values) are found in oxide-facies BIFs is exactly that predicted by DIR.

The range in Fe isotope compositions permitted by the model in Table 1 is very restricted because complete reduction of $Fe(OH)_3$ is assumed. The photic zone produced $Fe(OH)_3$ is assumed to have a δ^{56}Fe value of 0‰, which would reflect complete or near-complete oxidation of hydrothermal Fe^{2+}_{aq} via the pathways described by Eqs. (1) through (3), assuming a near-zero δ^{56}Fe value for hydrothermal Fe^{2+}_{aq} (Johnson et al., 2008b). Near-zero δ^{56}Fe values for $Fe(OH)_3$ would also be expected for detrital iron oxide/hydroxides (Beard et al., 2003b; Yamaguchi et al., 2005). Partial oxidation of hydrothermal Fe^{2+}_{aq} by any of the pathways described by Eqs. (1) through (3) would produce positive δ^{56}Fe values for $Fe(OH)_3$, most likely between ~0 and +1‰ (Bullen et al., 2001; Beard and Johnson, 2004; Croal et al., 2004), and this scenario would produce higher δ^{56}Fe values for siderite than those listed in Table 1. The slightly negative δ^{56}Fe values for siderite predicted by Eqs. (5) through (7) reflect isotopic equilibration between $FeCO_3$ and Fe^{2+}_{aq}, using the $^{56}Fe/^{54}Fe$ fractionation factor from Wiesli et al. (2004) and the mass-balance constraints imposed by the stoichiometry of the equations. The negative δ^{56}Fe values measured for siderite in the current study cannot be explained by complete reduction by DIR, nor can siderite that has positive δ^{56}Fe values be explained by complete reduction by DIR unless the precursor $Fe(OH)_3$ had positive δ^{56}Fe values, as noted above.

5.2.1. Other seawater components?

Eq. (4) requires significant C contributions from HCO_3^- from seawater and other elements could come from seawater. Rare earth elements (REE) and Y in carbonates, for example, are widely used as a proxy for seawater (e.g., Webb and Kamber, 2000; Kamber and Webb, 2001). The high sorption capacity of ferric hydroxides for REE + Y (e.g., Bau, 1999; Quinn et al., 2006a, b) raises the possibility that REE + Y released by microbial reduction of ferric oxide/hydroxides could contribute seawater-like compositions, although it is important to note that the experimentally determined REE + Y adsorption coefficients are variable. REE contents may be very high in pore fluids from sections of marine sediments that record microbial C and Fe cycling, and in some cases the REE patterns mimic those of seawater (e.g., Elderfield and Sholkovitz, 1987; Haley et al., 2004; Caetano et al., 2009). We conclude that, through a combination of direct contributions from seawater that accompanies seawater HCO_3^- addition, and release through microbial reduction of ferric hydroxides, REE + Y contents of DIR-generated Fe-rich carbonates could closely resemble those of seawater despite the fact that 100% of the Fe(II) might have been generated by DIR. Testing this possibility will require much larger sampling than that done in the current study, where mg-size samples were taken to maximize spatial selectivity, relative to the 100+ mg-size carbonate samples commonly used for REE + Y analyses.

In addition to trace element proxies for seawater, a logical question, given the expected high seawater Ca^{2+} and Mg^{2+} contents, is can DIR produce low-δ^{13}C Ca–Mg carbonates? Carbonate formation during DIR has been shown to mostly (but not entirely) exclude dissolved Ca^{2+} and Mg^{2+}, favoring siderite formation despite the presence of abundant dissolved alkaline earth ions (Mortimer et al., 1997; Roden et al., 2002). For siderite formation by DIR via Eqs. (5) through (7), decreasing quantities of seawater-derived HCO_3^- predict decreasing δ^{13}C values for siderite, and increasing quantities of Fe^{2+}_{aq}, under conditions of complete $Fe(OH)_3$ reduction (Table 1). If excess $Fe(OH)_3$ is present, free Fe^{2+}_{aq} would react to form magnetite (Eq. (8)), or, in the presence of silica, Fe silicates. The observation that the lowest δ^{13}C values for BIF siderite are found in oxide- and Fe silicate-facies BIFs (Fig. 5A) is exactly that expected for DIR.

5.3. Fe isotope evidence for multi-stage DIR

The average and median δ^{56}Fe values for BIF siderite analyzed in the current study are −0.03 and −0.07‰, respectively, suggesting that the overall Fe flux that generated the siderite layers had a near-zero δ^{56}Fe value. We interpret this to reflect the average Fe isotope composition of the flux of $Fe(OH)_3$ from the photic zone to the seafloor. This model follows that of Johnson et al. (2008a), who noted that magnetite and siderite from the ~2.5 Ga Dales Gorge Member of the Brockman Iron Formation, Australia, have an average δ^{56}Fe value near zero. If the $Fe(OH)_3$ flux to the seafloor had a δ^{56}Fe value near zero, and siderite did not generally form in Fe isotope equilibrium with seawater, then the range in δ^{56}Fe values measured for BIF siderite must reflect processes in the sediment, beneath the sediment/seawater interface, prior to lithification.

Partial microbial reduction of iron oxide produces Fe^{2+}_{aq} that has negative δ^{56}Fe values, reflecting isotopic fractionation between Fe^{2+}_{aq} and a reactive surface layer on the oxide substrate of −3 to −1‰ (Johnson et al., 2005; Crosby et al., 2005, 2007; Wu et al., 2009; Tangalos et al., in press). Assuming an average Fe^{2+}_{aq}-reactive iron oxide fractionation of −2‰, appropriate for a mixture of ferrihydrite and goethite (Tangalos et al., in press), reduction of 50% of the oxide substrate would, broadly speaking, produce Fe^{2+}_{aq} with a δ^{56}Fe value of ~−1‰. The remaining oxide would have a δ^{56}Fe value of ~+1‰, assuming simple mass balance and equilibrium conditions. Siderite that formed from DIR-generated Fe^{2+}_{aq} that was mobile in the sediment would be expected to be relatively free of inclusions of iron oxide substrate. In contrast, siderite that formed "in place" by reduction of the ferric oxide substrate could contain inclusions of residual iron oxide minerals if reduction did not quite go to completion. Siderites formed in this manner would be expected to have zero or positive δ^{56}Fe values, depending upon the extent of reduction that involved prior loss of low-δ^{56}Fe Fe^{2+}_{aq}. Our observation that siderites that contain iron oxide inclusions have δ^{56}Fe values ≥0‰ provides strong support for such a multi-step process of DIR in the soft sediment prior to lithification. Although they are a minor component in the Fe mass balance of the system (Figs. 5B and S3), these iron oxides are expected to have positive δ^{56}Fe values. Dehydration and phase transformation of residual ferric hydroxides is the best explanation for the presence of hematite and magnetite inclusions in these carbonates (e.g., Schwertmann and Cornell, 1991).

We illustrate the effects of variable extent of DIR in different locations in the soft-sediment section, along with mixing of variable C sources, in Fig. 6. Mixing of percolating Neoarchean/Paleoproterozoic seawater Fe (δ^{56}Fe ~0‰; 28 ppm, Ewers, 1980) and DIC (δ^{13}C ~0‰; 20 ppm, Holland, 1984), and end-member Fe and C isotope compositions derived from the reactions discussed above (Table 1), is shown by two sets of mixing lines. One set of lines shows the mixing of C with the lowest δ^{13}C value of ~−7.5‰ expected from reaction (4), in which the ratio of HCO_3^- derived from oxidation of CH_2O ($HCO_{3\,Org}^-$) to total HCO_3^- ($HCO_{3\,Total}^-$) = 1/4. In the second model, we consider a lower δ^{13}C value reflecting a greater component of $HCO_{3\,Org}^-$ ($HCO_{3\,Org}^-/HCO_{3\,Total}^- > 1/4$). Seawater Fe was mixed with Fe^{2+}_{aq} that had δ^{56}Fe values of ~−1‰, 0‰, and +1‰, as discussed above. Conceptually, these δ^{56}Fe values reflect partial DIR, complete DIR, and reduction of residual $Fe(OH)_3$ left over from partial DIR, respectively (points A, B, and C in Fig. 6). Combined, these mixing lines (see figure legend) produce C and Fe isotope compositions that encompass the range in measured δ^{13}C and δ^{56}Fe values, taking into account the Fe isotope effects of different degrees of DIR, Fe^{2+}_{aq} mobilization, and various ratios of $HCO_{3\,Org}^-$ to $HCO_{3\,Total}^-$.

A schematic view of the pathways involved in producing the observed δ^{13}C–δ^{56}Fe relations is shown in Fig. 7. Partial reduction of Fe $(OH)_3$ will produce Fe^{2+}_{aq} with a δ^{56}Fe of ~−1‰ or less if the extent of reduction is <50%. As highlighted by Johnson et al. (2008b), quasi-steady-state generation of low-δ^{56}Fe Fe^{2+}_{aq} could be sustained in sediments by a continual downward flux of $Fe(OH)_3$ and CH_2O

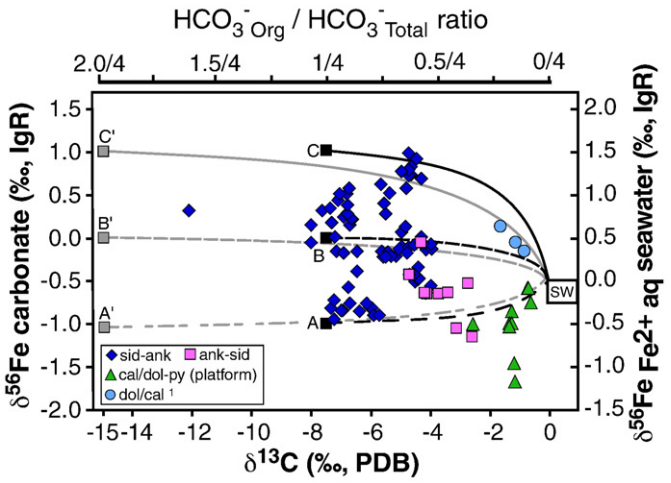

Fig. 6. Combined δ^{13}C (‰, PDB) and δ^{56}Fe (‰, igneous rocks) values measured in millimeter-scale samples of BIF and limestone/dolomite carbonates. The upper and lower X axes show $HCO_3^-{}_{Org}/HCO_3^-{}_{Total}$ ratios and δ^{13}C carbonate values, respectively, for mixing of organic matter-derived HCO_3^- with δ^{13}C = −30‰ (Beukes et al., 1990; Kaufman, 1996; Fischer et al., 2009) and seawater HCO_3^- with δ^{13}C ~0‰. A ratio of 1/4 (points A, B, and C) implies that the carbonate contains all the $HCO_3^-{}_{Org}$ produced by DIR (reaction (9)). Points A′, B′, and C′ indicate carbonates that contain a 2-fold higher amount of $HCO_3^-{}_{Org}$. Details of the δ^{13}C mixing calculations are given in Table S4. The δ^{56}Fe values for A, B, and C (−1‰, 0‰, and +1‰) reflect partial DIR, complete DIR, and the residue from partial DIR, respectively, of $Fe(OH)_3$ that had a δ^{56}Fe = 0‰. The lines represent mixing of C and Fe^{2+} with isotopic compositions A, B, and C (and A′, B′, and C′), with Archean/Proterozoic seawater compositions (28 ppm C and 20 ppm Fe; Holland, 1984; Ewers, 1980) of δ^{56}Fe = 0‰ and δ^{13}C = 0‰, to produce siderite with different proportions of DIR-derived Fe and C versus seawater Fe and C. The δ^{56}Fe scale on the *Y* axis to the right of the diagram corresponds to the δ^{56}Fe value of Fe^{2+}_{aq} in seawater in equilibrium with a given δ^{56}Fe value for carbonate calculated using the experimental Fe isotope fractionation factor of Wiesli et al. (2004) 1 is the same as in Fig. 5.

produced in the photic zone. Production of Fe^{2+}_{aq} and HCO_3^- with δ^{56}Fe ~−1‰ and δ^{13}C ~−30‰ via partial $Fe(OH)_3$ reduction is referred to as "stage 1" in Fig. 7. These mobile species may encounter HCO_3^- in seawater ($HCO_{3\,SW}^-$) in "stage 2" (Fig. 7), producing siderite that has δ^{56}Fe and δ^{13}C values of ~−1‰ and ~−7.5‰, respectively, via a reaction such as:

$$4Fe^{2+}_{aq} + HCO^-_{3\,Org} + 3HCO^-_{3\,SW} + 4OH^- \rightarrow 4FeCO_3 + 4H_2O. \quad (9)$$

BIF carbonates that have these Fe–C isotope compositions are plotted as "Group I" in the inset to Fig. 7; if additional $HCO_3^-{}_{SW}$ beyond the 3 mol required in Eq. (9) is provided from seawater, intermediate δ^{13}C values for carbonate may be produced via the mixing relations in Fig. 6.

The residual $Fe(OH)_3$ from partial reduction by DIR in "stage 1" should have positive δ^{56}Fe values, perhaps ~+1‰, based on isotopic mass balance, which is consistent with inferences from natural samples (Staubwasser et al., 2006). Further reduction of this residual $Fe(OH)_3$ would produce Fe–C isotope compositions that fall in the "Group II" data field in Fig. 7. Conversion of high-δ^{56}Fe $Fe(OH)_3$ to siderite by DIR requires additional HCO_3^- from seawater, which would result in siderite with δ^{56}Fe ~+1‰ and δ^{13}C ~−7.5‰. We label this pathway as "near-complete" reduction because of the common presence of micron-size ferric Fe-oxide (hematite, magnetite) inclusions in high-δ^{56}Fe siderites, a key petrographic indicator of DIR, as discussed above. We note that Pecoits et al. (2009) observed hematite inclusions in siderite from the Dales Gorge Member of the Brockman Iron Formation, Australia, and proposed that this relation reflected an oxide residue during siderite production through early sediment diagenesis by DIR.

6. Conclusions

The high abundance of siderite in Archean marine sedimentary rocks, including BIFs that were deposited below wave base, has provided

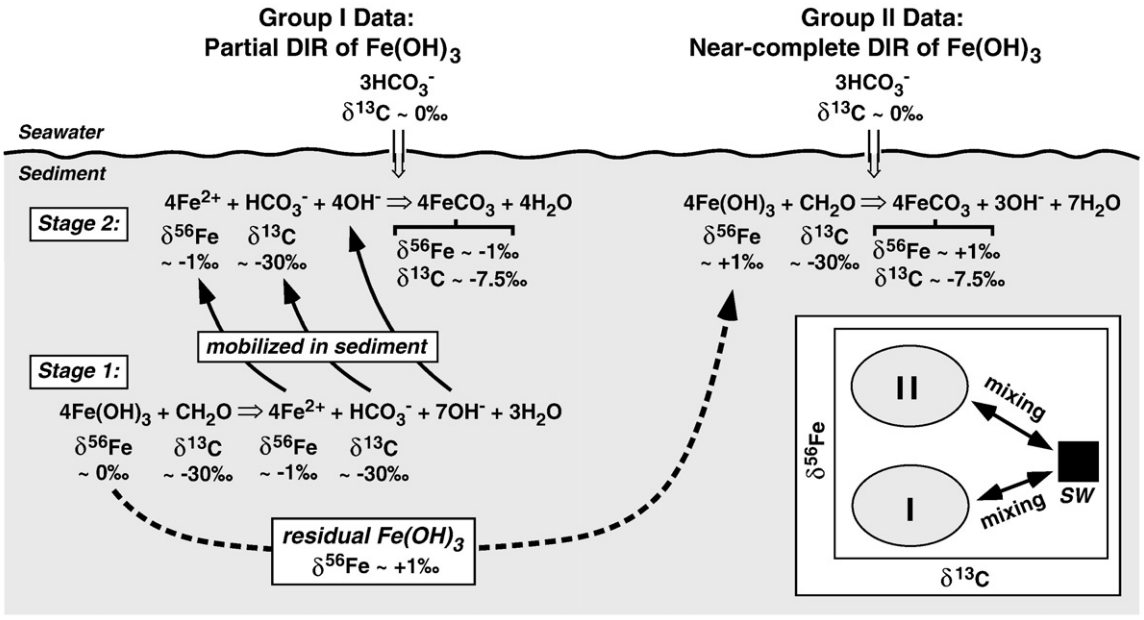

Fig. 7. Schematic diagram that shows a conceptual model for the diagenetic origin of BIF Fe carbonates based on mineralogical, chemical, and C, O, and Fe isotope data. Two main groups of carbonates that have low-$\delta^{13}C$ values (~ −7.5‰) are defined by low $\delta^{56}Fe$ values (~ −1‰; Group I) and high $\delta^{56}Fe$ values (~ +1‰; Group II), which originate through a multi-step process (see Section 5.3). For Group I data, in "stage 1," partial microbial reduction of $Fe(OH)_3$ with $\delta^{56}Fe$ of ~0‰ and oxidation of CH_2O with $\delta^{13}C$ ~ −30‰ results in generation of Fe^{2+}_{aq} with $\delta^{56}Fe$ ~ −1‰ and HCO_3^- with $\delta^{13}C$ ~ −30‰. In "stage 2," low−$\delta^{56}Fe$ Fe^{2+}_{aq} is mobilized and reacts elsewhere in the sediment column with (i) HCO_3^- derived from stage 1, and (ii) seawater HCO_3^- to form siderite with $\delta^{56}Fe$ ~ −1‰ and $\delta^{13}C$ ~ −7.5‰. Because Fe^{2+}_{aq} and HCO_3^- have been mobilized prior to Fe carbonate precipitation, Fe carbonates in this group do not contain Fe-oxide inclusions. Group II data are interpreted to reflect Fe^{2+}_{aq} produced by near-complete reduction of high-$\delta^{56}Fe$ residual $Fe(OH)_3$ from stage 1, which will produce siderite with $\delta^{56}Fe$ ~ +1‰ and $\delta^{13}C$ ~ −7.5‰. In this case, DIR and siderite formation are envisioned to occur "in place," and a small amount of un-reacted $Fe(OH)_3$ is later converted (by dehydration and recrystallization) to ferric oxide, forming hematite inclusions. This process is represented by carbonates that contain ferric oxide inclusions and fall in Group II of isotope compositions.

some of the most widely cited evidence for a stratified ocean that was anoxic and Fe^{2+}-rich in its deeper portions (e.g., Ohmoto et al., 2004; Tice and Lowe, 2004). The C, O, and Fe isotope data presented in this study, however, argue that virtually none of the siderites analyzed here from the ~2.5 Ga Kuruman Iron Formation formed in equilibrium with seawater and hence were not directly precipitated from the water column. This conclusion does not negate the hypothesis that the Archean oceans were Fe^{2+}-rich and contained abundant dissolved carbonate, but it does suggest that siderite may not be a direct proxy for ancient seawater. Given the evidence against significant stratification of $\delta^{13}C$ values for DIC in Neoarchean oceans, at least in the ~2.5 Ga Transvaal basin (Fischer et al., 2009), the common occurrence of negative $\delta^{13}C$ values for siderite in BIFs (e.g., Becker and Clayton, 1972; Perry et al., 1973; Thode and Goodwin, 1983; Beukes et al., 1990; Kaufman et al., 1990; Beukes and Klein, 1990; Winter and Knauth, 1992; Kaufman, 1996; Fischer et al., 2009) increasingly points to DIR as the major pathway for siderite formation in BIFs, as originally proposed by Walker (1984). Indeed, recent models for BIF formation have highlighted the likely role that DIR played in BIF formation (e.g., Konhauser et al., 2005; Beukes and Gutzmer, 2008; Fischer et al., 2009; Fischer and Knoll, 2009; Pecoits et al., 2009).

The relatively low $\delta^{18}O$ values of siderite in BIFs, as compared to the majority of broadly coeval Ca–Mg carbonates, has long posed a problem that may now be successfully explained by production of siderite largely through DIR. The ~9‰ range in $\delta^{18}O$ values for Campbellrand–Kuruman carbonates cannot be explained by differences in $^{18}O/^{16}O$ fractionation factors (e.g., O'Neil et al., 1969; Sheppard and Schwarcz, 1970; Carothers et al., 1988; Kim and O'Neil, 1997). Mortimer and Coleman (1997) highlighted the anomalously low $\delta^{18}O$ values in early diagenetic marine siderite, noting that DIR might explain this observation. The isotope mass-balance reactions presented here provide a solution to the long-standing problem that the $\delta^{13}C$ and $\delta^{18}O$ values for BIF siderite are too low relative to those expected for precipitation from seawater, and we propose that the $\delta^{13}C$ and $\delta^{18}O$ values of BIF siderite reflect direct inheritance of C and O isotope compositions of the precursor organic carbon and iron oxide. These reactions can also explain the contrast in C and O isotope compositions of siderite from oxide- and Fe silicate-facies BIFs relative to siderite-facies BIFs, an observation that has been relatively ignored in the literature.

The wide range in $\delta^{56}Fe$ values for siderite from the Kuruman Iron Formation indicates that few siderites were in Fe isotope equilibrium with seawater, but instead records authigenic and early diagenetic mineral formation in the soft sediment prior to lithification. Simple flux models demonstrate that the oceans may become stratified in $\delta^{56}Fe$ values through processes such as extensive oxide precipitation in the photic zone, but this stratification can only occur if the photic zone contains very low dissolved Fe contents (Johnson et al., 2008a), and such environments cannot produce extensive deposition of Fe-rich carbonates. We therefore draw an important distinction between Ca–Mg carbonates whose Fe isotope compositions may directly reflect those of seawater (e.g., von Blanckenburg et al., 2008; Czaja et al., 2010) and the Fe-rich carbonates that are the focus of the current study.

It is understandable that the debates on the cause of the Fe isotope signals recorded in Neoarchean and Paleoproterozoic marine sedimentary rocks has focused on the samples that have negative $\delta^{56}Fe$ values, because these deviate most strongly from the near-zero $\delta^{56}Fe$ values that characterize the continental and oceanic crust, detrital Fe loads, and hydrothermal Fe fluxes. The results from the current study, however, indicate that the inventory of Fe that has negative $\delta^{56}Fe$ values may be but a small fraction of that cycled by low-temperature biological processes during this time. BIFs are particularly valuable in assessing the quantities of Fe that may have been biologically cycled in ancient marine environments because the combination of their very high Fe contents and non-zero $\delta^{56}Fe$ values are very difficult to explain through abiological redox processes such as extensive oxide precipitation (Johnson et al., 2008b). The Fe isotope data presented

here, when considered in light of C and O isotope compositions determined on the same samples, indicate that authigenic and early diagenetic minerals that have negative, near-zero, or even positive δ^{56}Fe values may also record biological cycling, demonstrating that a complete understanding of the extent of biological versus abiological Fe cycling requires multiple lines of evidence and careful petrographic sample characterization.

Acknowledgements

We thank John Fournelle for his help with electron microprobe, SEM, and EBSD determinations and Hiromi Konishi and Huifang Xu for performing preliminary TEM analysis. We thank Max Coleman for useful discussions. Journal reviews by editor Rick Carlson, Balz Kamber, and an anonymous reviewer helped to improve the manuscript. This research was funded by the NASA Astrobiology Institute and the National Science Foundation.

Appendix A. Supplementary data

Supplementary data associated with this article can be found, in the online version, at doi:10.1016/j.epsl.2010.02.015.

References

Altermann, W., Nelson, D.R., 1998. Sedimentation rates, basin analysis and regional correlations of three Neoarchean and Palaeoproterozoic sub-basins of the Kaapvaal craton as inferred from precise U–Pb zircon ages from volcaniclastic sediments. Sed. Geol. 120, 225–256.

Anbar, A.D., Rouxel, O., 2007. Metal stable isotopes in paleoceanography. Ann. Rev. Earth Planet. Sci. 35, 717–746.

Anbar, A.D., Jarzecki, A.A., Spiro, T.G., 2005. Theoretical investigation of iron isotope fractionation between $Fe(H_2O)_6^{3+}$ and $Fe(H_2O)_6^{2+}$; implications for iron stable isotope geochemistry. Geochim. Cosmochim. Acta 69, 825–837.

Archer, C., Vance, D., 2006. Coupled Fe and S isotope evidence for Archean microbial Fe(III) and sulfate reduction. Geology 34, 153–156.

Bao, H., Koch, P.L., 1999. Oxygen isotope fractionation in ferric oxide-water systems; low temperature synthesis. Geochim. Cosmochim. Acta 63, 599–613.

Bao, H., Koch, P.L., Thiemens, M.H., 2000. Oxygen isotopic composition of ferric oxides from Recent soil, hydrologic, and marine environments. Geochim. Cosmochim. Acta 64, 2221–2231.

Bau, M., 1999. Scavenging of dissolved yttrium and rare earths by precipitating iron oxyhydroxide: experimental evidence for Ce oxidation, Y–Ho fractionation, and lanthanide tetrad effect. Geochim. Cosmochim. Acta 63, 67–77.

Baur, M.E., Hayes, J.M., Studley, S.A., Walter, M.R., 1985. Millimeter-scale variations of stable isotope abundances in carbonates from banded iron formations in the Hamersley Group of Western Australia. Econ. Geol. 80, 270–282.

Beard, B.L., Johnson, C.M., 2004. Fe isotope variations in the modern and ancient Earth and other planetary bodies. In: Johnson, C.M., Beard, B.L., Albarede, F. (Eds.), Reviews in Mineralogy and Geochemistry: Geochemistry of Non-Traditional Stable Isotopes: Min. Soc. Am., 55, pp. 319–357.

Beard, B.L., Johnson, C.M., Skulan, J.L., Nealson, K.H., Cox, L., Sun, H., 2003a. Application of Fe isotopes to tracing the geochemical and biological cycling of Fe. Chem. Geol. 195, 87–117.

Beard, B.L., Johnson, C.M., Von Damm, K.L., Poulson, R.L., 2003b. Iron isotope constraints on Fe cycling and mass balance in oxygenated Earth oceans. Geology 31, 629–632.

Beck, W.C., Grossman, E.L., Morse, J.W., 2005. Experimental studies of oxygen isotope fractionation in the carbonic acid system at 15 °C, 25 °C, and 40 °C. Geochim. Cosmochim. Acta 69, 3493–3503.

Becker, R.H., Clayton, R.N., 1972. Carbon isotopic evidence for the origin of a banded iron-formation in Western Australia. Geochim. Cosmochim. Acta 36, 577–595.

Beukes, N.J., Gutzmer, J., 2008. Origin and paleoenvironmental significance of major iron formations at the Archean-Paleoproterozoic boundary. Soc. Econ. Geol. Rev. 15, 5–47.

Beukes, N.J., Klein, C., 1990. Geochemistry and sedimentology of a facies transition, from microbanded to granular iron-formation, in the early Proterozoic Transvaal Supergroup, South Africa. Precamb. Res. 47, 99–139.

Beukes, N.J., Klein, C., Kaufman, A.J., Hayes, J.M., 1990. Carbonate petrography, kerogen distribution, and carbon and oxygen isotope variations in an early Proterozoic transition from limestone to iron-formation deposition, Transvaal Supergroup, South Africa. Econ. Geol. 85, 663–690.

Bullen, T.D., White, A.F., Childs, C.W., Vivit, D.V., Schulz, M.S., 2001. Demonstration of significant abiotic iron isotope fractionation in nature. Geology 29, 699–702.

Caetano, M., Prego, R., Vale, C., de Pablo, H., Marmolejo-Rodríguez, J., 2009. Record of diagenesis of rare earth elements and other metals in a transitional sedimentary environment. Marine Chem. 116, 36–46.

Cairns-Smith, A.G., 1978. Precambrian solution photochemistry, inverse segregation, and banded iron formations. Nature 276, 807–808.

Carothers, W.W., Adami, L.H., Rosenbauer, R.J., 1988. Experimental oxygen isotope fractionation between siderite–water and phosphoric acid liberated CO_2–siderite. Geochim. Cosmochim. Acta 52, 2445–2450.

Cheney, E.S., 1996. Sequence stratigraphy and plate tectonic significance of the Transvaal succession of Southern Africa and its equivalent in Western Australia. Precamb. Res. 79, 3–24.

Cloud, P., 1968. Atmospheric and hydrospheric evolution on the primitive earth. Science 160, 729–736.

Croal, L., Johnson, C.M., Beard, B.L., Newman, D.K., 2004. Iron isotope fractionation by Fe(II)-oxidizing photoautotrophic bacteria. Geochim. Cosmochim. Acta 68, 1227–1242.

Crosby, H.A., Johnson, C.M., Roden, E.E., Beard, B.L., 2005. Coupled Fe(II)–Fe(III) electron and atom exchange as a mechanism for Fe isotope fractionation during dissimilatory iron oxide reduction. Environ. Sci. Technol. 39, 6698–6704.

Crosby, H.A., Roden, E.E., Johnson, C.M., Beard, B.L., 2007. The mechanisms of iron isotope fractionation produced during dissimilatory Fe(III) reduction by Shewanella putrefaciens and Geobacter sulfurreducens. Geobiology 5, 169–189.

Czaja, A.D., Johnson, C.M., Beard, B.L., Eigenbrode, J.L., Freeman, K.H., Yamaguchi, K.E., 2010. Iron and carbon isotope evidence for ecosystem and environmental diversity in the ~2.7 to 2.5 Ga Hamersley Province, Western Australia. Earth Planet. Sci. Letters. 292, 170–180.

Domagal-Goldman, S.D., Kubicki, J.D., 2008. Density functional theory predictions of equilibrium isotope fractionation of iron due to redox changes and organic complexation. Geochim. Cosmochim. Acta 72 (21), 5201–5216.

Elderfield, H., Sholkovitz, E.R., 1987. Rare earth elements in the pore waters of reducing nearshore sediments. Earth Planet. Sci. Letters 82, 280–288.

Ewers, W.E., 1980. Chemical conditions for the precipitation of banded iron-formations. Biogeochemistry of Ancient and Modern Environments, Eds. P.A. Trudinger, Walter, M.R., and Ralph, B.J. Springer-Verlag, Netley, Australia, pp. 83–92.

Fischer, W.W., Knoll, A.H., 2009. An iron shuttle for deep-water silica in Late Archean and Early Paleoproterozoic iron formation. Geol. Soc. Am. Bull. 121, 222–235.

Fischer, W.W., Schroeder, S., Lacassie, J.P., Beukes, N.J., Goldberg, T., Strauss, H., Horstmann, U.E., Schrag, D.P., Knoll, A.H., 2009. Isotopic constraints on the Late Archean carbon cycle from the Transvaal Supergroup along the western margin of the Kaapvaal Craton, South Africa. Precamb. Res. 169, 15–27.

Guy, R.D., Fogel, M., Berry, J.A., 1993. Photosynthetic fractionation of the stable isotopes of oxygen and carbon. Plant Physiol. 101, 37–47.

Haley, B.A., Klinkhammer, G.P., McManus, J., 2004. Rare earth elements in pore waters of marine sediments. Geochim. Cosmochim. Acta 68, 1265–1279.

Holland, H.D., 1984. The Chemical Evolution of the Atmosphere and Oceans. Princeton University Press, Princeton, N.J.

Jimenez-Lopez, C., Romanek, C.S., 2004. Precipitation kinetics and carbon isotope partitioning of inorganic siderite at 25 ºC and 1 atm. Geochim. Cosmochim. Acta 68, 557–571.

Jimenez-Lopez, C., Caballero, E., Huertas, F.J., Romanek, C.S., 2001. Chemical, mineralogical and isotope behavior, and phase transformation during the precipitation of calcium carbonate minerals from intermediate ionic solution at 25 ºC. Geochim. Cosmochim. Acta 65, 3219–3231.

Johnson, C.M., Beard, B.L., Beukes, N.J., Klein, C., O'Leary, J.M., 2003. Ancient geochemical cycling in the Earth as inferred from Fe isotope studies of banded iron formations from the Transvaal Craton. Contrib. Mineral. Petrol. 144, 523–547.

Johnson, C.M., Roden, E.E., Welch, S.A., Beard, B.L., 2005. Experimental constraints on Fe isotope fractionation during magnetite and Fe carbonate formation coupled to dissimilatory hydrous ferric oxide reduction. Geochim. Cosmochim. Acta 69, 963–993.

Johnson, C.M., Beard, B.L., Klein, C., Beukes, N.J., Roden, E.E., 2008a. Iron isotopes constrain biologic and abiologic processes in banded iron formation genesis. Geochim. Cosmochim. Acta 72, 151–169.

Johnson, C.M., Beard, B.L., Roden, E.E., 2008b. The iron isotope fingerprints of redox and biogeochemical cycling in modern and ancient Earth. Ann. Rev. Earth Planet. Sci. 36, 457–493.

Kamber, B.S., Webb, G.E., 2001. The geochemistry of late Archean microbial carbonate: implications for ocean chemistry and continental history. Geochim. Cosmochim. Acta 65, 2509–2525.

Kamber, B.S., Whitehouse, M.J., 2007. Micro-scale sulphur isotope evidence for sulphur cycling in the late Archean shallow ocean. Geobiology 5, 5–17.

Kappler, A., Pasquero, C., Konhauser, K.O., Newman, D.K., 2005. Deposition of banded iron formations by anoxygenic phototrophic Fe(II)-oxidizing bacteria. Geology 33, 865–868.

Kasting, J.F., Howard, M.T., Wallman, K., Veizer, J., Shields, G.A., Jaffrés, J., 2006. Paleoclimates, ocean depth, and the oxygen isotopic composition of seawater. Earth Planet. Sci. Lett. 252, 82–93.

Kaufman, A.J., 1996. Geochemical and mineralogic effects of contact metamorphism on banded iron-formation: an example from the Transvaal Basin, South Africa. Precamb. Res. 79, 171–194.

Kaufman, A.J., Hayes, J.M., Klein, C., 1990. Primary and diagenetic controls of isotopic compositions of iron-formation carbonates. Geochim. Cosmochim. Acta 54, 3461–3473.

Kim, S.-T., O'Neil, J.R., 1997. Equilibrium and nonequilibrium oxygen isotope effects in synthetic carbonates. Geochim. Cosmochim. Acta 61, 3461–3475.

Klein, C., 2005. Some Precambrian banded iron-formations (BIFs) from around the world: their age, geologic setting, mineralogy, metamorphism, geochemistry, and origin. Am. Mineral. 90, 1473–1499.

Klein, C., Beukes, N.J., 1989. Geochemistry and sedimentology of a facies transition from limestone to iron-formation deposition in the early proterozoic Transvaal Supergroup. South-Africa. Econ. Geol. 84, 1733–1774.

Knauth, L.P., 2005. Temperature and salinity history of the Precambrian ocean: implications for the course of microbial evolution. Palaeog., Palaeoclimat. Palaeoec. 219, 53–69.
Konhauser, K.O., Hamade, T., Raiswell, R., Morris, R.C., Ferris, F.G., Southam, G., Canfield, D.E., 2002. Could bacteria have formed the Precambrian banded iron formations? Geology 30, 1079–1082.
Konhauser, K.O., Newman, D.K., Kappler, A., 2005. The potential significance of microbial Fe(III) reduction during deposition of Precambrian banded iron formations. Geobiology 3, 167–177.
Konhauser, K., Lalonde, S., Amskold, L., Posth, N., Kappler, A., Anbar, A., 2007. Decoupling photochemical Fe(II) oxidation from shallow-water BIF deposition. Geochim. Cosmochim. Acta 71, A509.
Lovley, D.R., 1991. Dissimilatory Fe(III) and Mn(IV) reduction. Microbiol. Rev. 55, 259–287.
Lovley, D.R., 2004. Potential role of dissimilatory iron reduction in the early evolution of microbial respiration. In: Seckbach, J. (Ed.), Origins, Evolution, and Biodiversity of Microbial Life. Kluwer, Netherlands, pp. 301–313.
Lovley, D.R., Stolz, J.F., Nord, G.L., Phillips, E.J.P., 1987. Anaerobic production of magnetite by a dissimilatory iron-reducing microorganism. Nature 330, 252–254.
Miyano, T., Beukes, N.J., 1984. Phase relations of stilpnomelane, ferriannite and riebeckite in very low-grade metamorphosed iron-formations. Geol. Soc. South Africa Trans. 87, 111–124.
Mortimer, R.J.G., Coleman, M.L., 1997. Microbial influence on the oxygen isotope composition of diagenetic siderite. Geochem. Cosmochim. Acta 61, 1705–1711.
Mortimer, R.J.G., Coleman, M.L., Rae, J.E., 1997. Effect of bacteria on the elemental composition of early diagenetic siderite: implications for palaeoenvironmental interpretations. Sediment. 44, 759–765.
Muehlenbachs, K., 1998. The oxygen isotopic composition of the oceans, sediments and the seafloor. Chem. Geol. 145, 263–273.
Nealson, K.H., Myers, C.R., 1990. Iron reduction by bacteria: a potential role in the genesis of banded iron formations. Am. J. Sci. 290, 35–45.
O'Neil, J.R., Clayton, R.N., Mayeda, T.K., 1969. Oxygen isotope fractionation in divalent metal carbonates. J. Chem. Phys. 12, 5547–5558.
Ohmoto, H., Watanabe, Y., Kumazawa, K., 2004. Evidence from massive siderite beds for a CO_2-rich atmosphere before ~1.8 billion years ago. Nature 429, 395–399.
Pecoits, E., Gingras, M.K., Barley, M.E., Kappler, A., Posth, N.R., Konhauser, K.O., 2009. Petrography and geochemistry of the Dales Gorge banded iron formation: paragenetic sequence, source and implications for palaeo-ocean chemistry. Precamb. Res. 172, 163–187.
Perry, E.C., Tan, F.C., Morey, G.B., 1973. Geology and stable isotope geochemistry of the Biwabik iron formation, northern Minnesota. Econ. Geol. 68, 1110–1125.
Polyakov, V.B., Mineev, S.D., 2000. The use of Moessbauer spectroscopy in stable isotope geochemistry. Geochim. Cosmochim. Acta 64, 849–865.
Quinn, K.A., Byrne, R.H., Schijf, J., 2006a. Sorption of yttrium and rare earth elements by amorphous ferric hydroxide; influence of solution complexation with carbonate. Geochim. Cosmochim. Acta 70, 4151–4165.
Quinn, K.A., Byrne, R.H., Schijf, J., 2006b. Sorption of yttrium and rare earth elements by amorphous ferric hydroxide: influence of pH and ionic strength. Marine Chem. 99, 128–150.
Roden, E.E., Leonardo, M.R., Ferris, F.G., 2002. Immobilization of strontium during iron biomineralization coupled to dissimilatory hydrous ferric oxide reduction. Geochim. Cosmochim. Acta 66, 2823–2839.
Rouxel, O.J., Bekker, A., Edwards, K.L., 2005. Iron isotope constraints on the Archean and Paleoproterozoic ocean redox state. Science 307, 1088–1091.
Schauble, E.A., Rossman, G.R., Taylor, H.P., 2001. Theoretical estimates of equilibrium Fe-isotope fractionations from vibrational spectroscopy. Geochim. Cosmochim. Acta 65, 2487–2497.
Schwertmann, U., Cornell, R.M., 1991. Iron Oxides in the Laboratory; Preparation and Characterization. VCH, Weinheim, Federal Republic of Germany. 137p.
Sheppard, S.M.F., Schwarcz, H.P., 1970. Fractionation of carbon and oxygen isotopes and magnesium between coexisting metamorphic calcite and dolomite. Contrib. Min. Petrol. 26, 161–198.
Shields, G., Veizer, J., 2002. Precambrian marine carbonate isotope database: version 1.1. Geochem. Geophys. Geosyst. G3, 3. doi:10.1029/2001GC000266.
Staubwasser, M., von Blanckenburg, F., Schoenberg, R., 2006. Iron isotopes in the early marine diagenetic iron cycle. Geology 34 (8), 629–632.
Swart, P.K., 1991. The oxygen and hydrogen isotopic composition of the Black Sea. Deep-Sea Res. 38 (2), S761–S772.
Tangalos, G.E., Beard, B.L., Johnson, C.M., Alpers, C.N., Shelobolina, E.S., Xu, H., Konishi, H., Roden, E.E., in press. Microbial production of isotopically light iron(II) in a modern chemically precipitated sediment and implications for isotopic variations in ancient rocks. Geobiology. doi:10.1111/j.1472-4669.2010.00237.x.
Thode, H.G., Goodwin, A.M., 1983. Further sulfur and carbon isotope studies of late Archean iron-formations of the Canadian shield and the rise of sulfate reducing bacteria. Precamb. Res. 20, 337–356.
Tice, M.M., Lowe, D.R., 2004. Photosynthetic microbial mats in the 3,416-Myr-old ocean. Nature 431, 549–552.
Trendall, A.F., 2002. The significance of iron-formation in the Precambrian stratigraphic record. In: Altermann, W., Corcorane, P.L. (Eds.), Precambrian Sedimentary Environments: A Modern Approach to Depositional Systems: International Association of Sedimentologists Special Publication, vol 44, pp. 33–66.
Trendall, A.F., Compston, W., Nelson, D.R., De Laeter, J.R., Bennett, V.C., 2004. SHRIMP zircon ages constraining the depositional chronology of the Hamersley Group, Western Australia. Aust. J. Earth Sci. 51, 621–644.
Vargas, M., Kashefi, K., Blunt-Harris, E.L., Lovley, D.R., 1998. Microbiological evidence for Fe(III) reduction on early Earth. Nature 395, 65–67.
von Blanckenburg, F., Mamberti, M., Schoenberg, R., Kamber, B.S., Webb, G.E., 2008. The iron isotope composition of microbial carbonate. Chem. Geol. 249, 113–128.
Walker, J.C.G., 1984. Suboxic diagenesis in banded iron formations. Nature 309, 340–342.
Webb, G.E., Kamber, B.S., 2000. Rare earth elements in Holocene reefal microbialites: implications for ancient seawater proxies. Geochim. Cosmochim. Acta 64, 1557–1565.
Wiesli, R.A., Beard, B.L., Johnson, C.M., 2004. Experimental determination of Fe isotope fractionation between aqueous Fe(II), siderite and “green rust” in abiotic systems. Chem. Geol. 211, 343–362.
Winter, B.L., Knauth, L.P., 1992. Stable isotope geochemistry of cherts and carbonates from the 2.0 Ga Gunflint iron formation: implications for the depositional setting, and the effects of diagenesis and metamorphism. Precamb. Res. 59, 283–313.
Wu, L., Beard, B.L., Roden, E.E., Johnson, C.M., 2009. Influence of pH and dissolved Si on Fe isotope fractionation during dissimilatory microbial reduction of hematite. Geochim. Cosmochim. Acta 73, 5584–5599.
Yamaguchi, K.E., Johnson, C.M., Beard, B.L., Ohmoto, H., 2005. Biogeochemical cycling of iron in the Archean-Paleoproterozoic Earth: constraints from iron isotope variations in sedimentary rocks from the Kaapvaal and Pilbara Cratons. Chem. Geol. 218, 135–169.